Journal of
Instrumentation

X-ray scattering tensor tomography with a random wavefront modulator to study 3D microstructures in archaeological skeletal remains

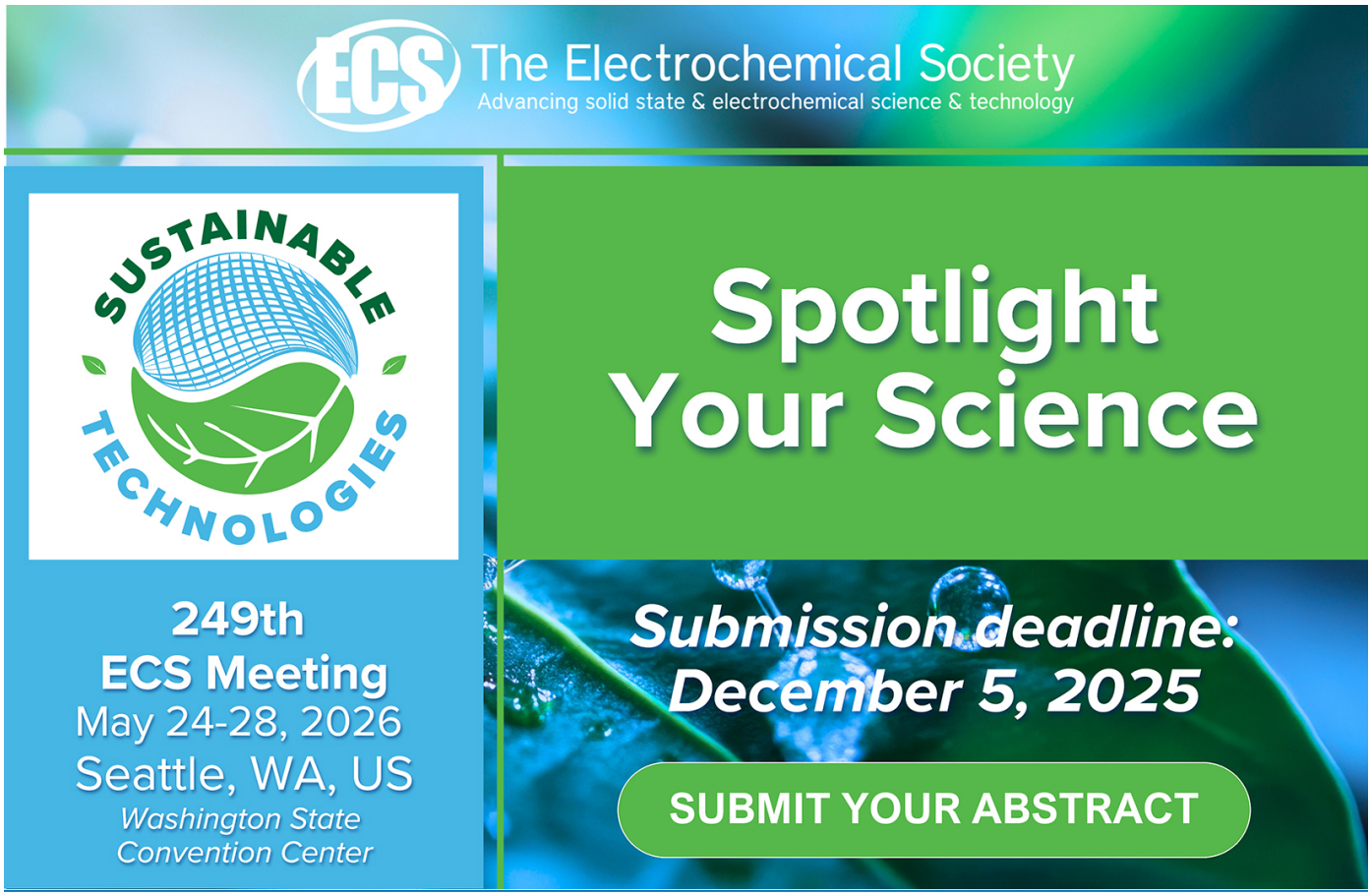

Published by IOP Publishing for Sissa Medialab

Received: *November 29, 2024*
Revised: *January 6, 2025*
Accepted: *January 19, 2025*
Published: *February 13, 2025*

25th International Workshop on Radiation Imaging Detectors
Lisbon, Portugal
30 June – 4 July 2024

X-ray scattering tensor tomography with a random wavefront modulator to study 3D microstructures in archaeological skeletal remains

Ginevra Lautizi[a,b,*], **Simone A.M. Lemmers**[b], **Vittorio Di Trapani**[a,b], **Margaux Schmeltz**[c], **Marie-Christine Zdora**[d], **Ludovic Broche**[e], **Alain Studer**[f], **Federica Marone**[c], **Marco Stampanoni**[c,g] and **Pierre Thibault**[a,b]

[a] *Department of Physics, University of Trieste, Trieste 34127, Italy*
[b] *Elettra-Sincrotrone Trieste, Basovizza 34149, Italy*
[c] *Swiss Light Source, Paul Scherrer Institut, Villigen 5232, Switzerland*
[d] *School of Physics and Astronomy, Monash University, Clayton Campus, Melbourne, VIC 3800, Australia*
[e] *ESRF, The European Synchrotron, Grenoble 38043 Cedex 9, France*
[f] *Data Processing Development and Consulting Group, Paul Scherrer Institut, Villigen 5232, Switzerland*
[g] *Institute for Biomedical Engineering, ETH Zürich, Zürich 8092, Switzerland*

E-mail: ginevra.lautizi@phd.units.it

Abstract: We present an application of X-ray scattering tensor tomography with a random wavefront modulator to resolve the orientation of microstructures in archaeological skeletal remains. We experimentally investigated two fragments from different tissue types — cortical bone and a root dentine — commonly analyzed in archaeological and palaeoanthropological research. This study hints at the potential to advance methodologies for both archaeological research and clinical applications.

Keywords: Computerized Tomography (CT) and Computed Radiography (CR); Data processing methods; Image reconstruction in medical imaging; Inspection with x-rays

*Corresponding author.

https://doi.org/10.1088/1748-0221/20/02/C02028

Contents

2025 JINST 20 C02028

1 Introduction

Small-angle X-ray scattering, often referred to as dark-field signal, gives sub-micron length-scale information about the structures in non-crystalline macroscopic samples, often not resolvable with conventional approaches such as micro-CT [1–3]. The directionality of the dark-field signal can also be extracted, enabling a reliable reconstruction of both the local angle and the extent of orientation of sample structures, which is the subject of ongoing research [4–7]. Since access to the scattering information is not directly limited by the spatial resolution of the system, it is possible to determine the local angle and the degree of orientation of structures smaller than the system's resolution.

In X-ray tensor tomography, two-dimensional projection images, with small-angle scattering signals, are acquired at various orientations of the sample. The two-dimensional directional scattering signals can be combined to reconstruct tomographically the local scattering tensor of the sample [7–9]. To this end, our group has recently made an important step forward with a new signal extraction method that provides directional dark-field information [10, 11]. Our general reconstruction method is applicable to data obtained using different wavefront modulators to reconstruct tensor tomography volumes.

In biological samples such as bones and teeth, the scattering signal can provide valuable insights into the microstructural arrangement of components like collagen fibers or dentinal tubules, with a centimeter-scale field of view. In this manuscript, we present a tensor tomography experiment conducted at the ID19-ESRF beamline in Grenoble, where we experimentally investigated two fragments from different tissue types — cortical bone and a root dentine — commonly analyzed in archaeological and palaeoanthropological research.

In the archaeological tooth sample, dentine tubules — microscopic, hollow channels extending from the pulp chamber to the outer dentine surface — were of particular interest. Filled with fluid and containing extensions of odontoblast cells, these tubules are more densely packed and wider near the pulp, gradually becoming sparser and narrower towards the enamel-dentine junction. Their directional organization plays a key role in the mechanical properties of the dentine, influencing its response to stress and wear. Their orientation offers insights into functional adaptations, such as how teeth evolved to accommodate different diets or chewing forces, and may also indicate stress or developmental disruptions during growth [12, 13].

Similarly, in the archaeological bone sample, the focus was on the orientation of collagen fibers within the bone matrix, which is crucial for the bone's strength and flexibility. Collagen fibers in bone can exhibit two patterns: disorganized in woven bone, or highly organized in lamellar bone. Woven bone, typically found in newly forming or healing bone, has randomly arranged collagen fibers, providing quick but temporary strength. In contrast, lamellar bone has a more orderly structure, with parallel fibers arranged in layers within osteons, offering greater durability and mechanical stability. The alignment of these fibers plays a critical role in the bone's ability to withstand forces and distribute stress, influencing its overall structure and function during growth, repair, and regular activity.

By examining these two samples, this study aims to give a first insight into whether tensor tomography can resolve the orientation of fibers in these tissues, potentially advancing methodologies for studying archaeological human remains.

2 Materials and methods

2.1 Experimental setup

X-ray tensor tomography with a sandpaper modulator was performed at the ID19-ESRF beamline. We used the U13 undulator (bandwidth = 1%) in combination with 2.8 mm of aluminum filter to obtain a mean energy of 26.5 keV. As a wavefront modulator, we used a diffuser made of 6 sheets of *P*180 grit silicon-carbide sandpaper. As a detector, we used a PCO.edge sCMOS detector coupled to a LuAG:Ce scintillator and a coupled objective, featuring a pixel size of 6.5 µm. The diffuser-sample distance was 0.89 m, while the sample-detector distance was 0.88 m. The total FOV was 1650 × 1570 pixel or 10.7 mm × 10.2 mm. An outline of the experimental setup is shown in figure 1.

To acquire the images, we followed the stair-wise acquisition protocol described in [7, 8]. For each tilt angle β, we acquired 400 projections with a continuous rotation of the sample over 360°, while β ranged from 0° to 45° with an angular step of 15°.

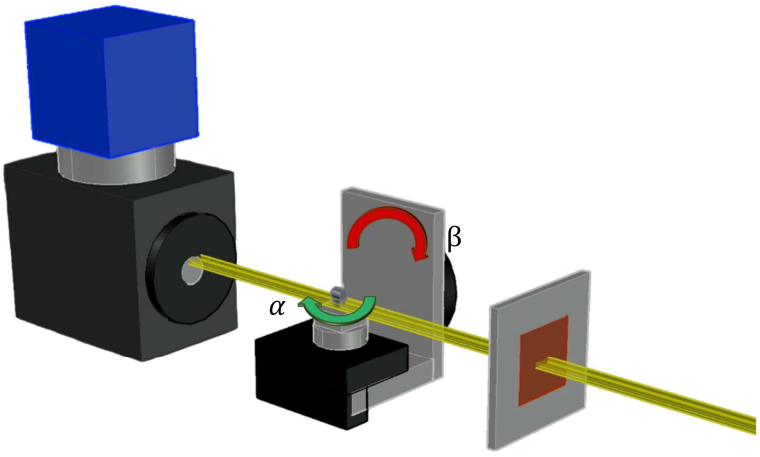

Figure 1. Schematic overview of the experimental setup. The X-ray beam is modulated by a diffuser mounted on a scanning stage upstream of the tilt and rotation stages. The rotation motor revolves α degrees and the rotation axis can be tilted β degrees. The detector system consists of a sCMOS camera.

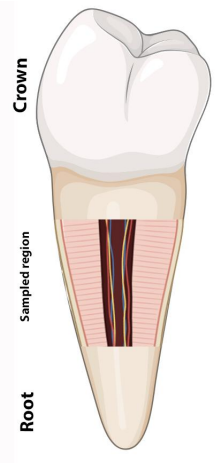

Figure 2. An outline of the sampled region of the analyzed permanent premolar.

2025 JINST 20 C02028

2.2 Visibility analysis of the modulator

To characterize the performance of the modulator, we calculated its visibility and mean speckle size. In figure 3a a flat-corrected reference image is shown, together with its visibility analysis. The visibility is determined as the ratio of the standard deviation to the mean intensity value of the reference image. The visibility map is then computed using a Gaussian filter, with a kernel size of 5 pixels. The visibility map is shown in figure 3b, where the mean visibility is 17%.

In figure 3c-d the mean speckle size of the modulator is shown, which is determined by calculating the full width at half maximum (FWHM) of the radial profile from the 2D auto-correlation function of a reference image. The speckle size is estimated to be 6.5 pixel, which correspond to 42.2 µm.

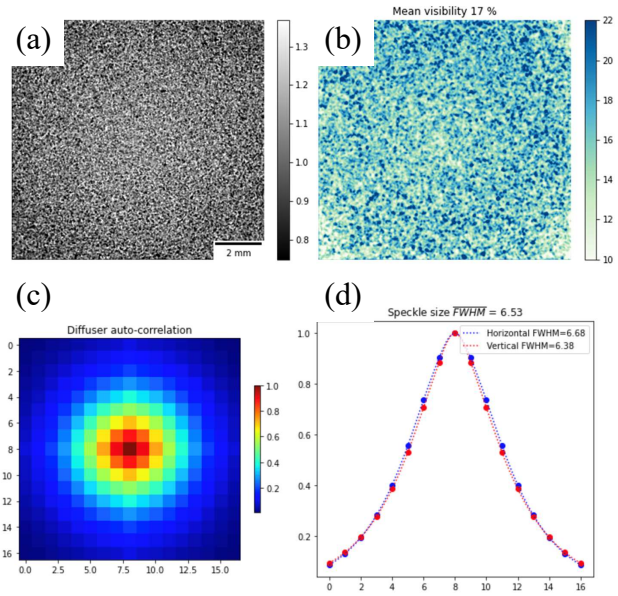

Figure 3. A flat-corrected reference image in gray levels (a) and (b) its visibility analysis in terms of percentage. In (c) a 3D representation of the speckle size auto-correlation function and in (d) its radial profile as normalized intensity vs. pixel coordinates.

2.3 Sample preparation

The samples used in this study were remnants of histological sections prepared for ref. [14], originating from a historical cemetery. These fragments were control samples for a project focused on examining bioerosion and the preservation state of skeletal remains after heat exposure. All skeletal remains are from adult individuals, although no additional life history data was available. The selected bone sample concerns a femur anterior midshaft cortical bone fragment. The dental sample concerns a root fragment of a permanent premolar. Both fragments, despite being archaeological in origin, were in a good preservation state with minimal signs of microbial damage.

3 Results

The acquired projections were analyzed with the reconstruction method presented in refs. [10, 11]. For both archaeological samples, we used as analysis window a 10×10 pixels square translated

2025 JINST 20 C02028

by 5 pixels, with a resulting spatial resolution of 32.5 µm. This window is a good compromise between a high spatial resolution and a low noise level in the reconstructed images. The computation time also plays a role in the decision of a proper analysis window. With this analysis window, the computation time for a single projection was 50 s.

For each analysis window, the 2D scattering tensor is calculated [10, 11] and eigendecomposed. Given the eigenvalues of the scattering tensor for each voxel, the following quantities can be derived. The mean of the eigenvalues represents the mean scattering within a defined window. The fractional anisotropy (FA) [15] indicates the degree of fiber alignment within the window. Regions with a high volume fraction of well-aligned fibers will display elevated FA values. The eigenvector corresponding to the smallest eigenvalue signifies the preferential local fiber orientation. We will show the above-mentioned quantities, as indicators for assessing the level of fiber scattering, alignment, and orientation.

For both samples, the omnidirectional dark-field signal was extracted from each projection of the tomographic dataset. The tensor sinogram was created by combining these results to determine the entire 3D scattering tensor field. A modified version of the alignment procedure from [2] was used to align the projections. Since the local structure-orientation signal is sensitive to noise, especially in background areas and at sharp edges, a threshold-based mask based on attenuation was applied to the tomographic volumes of fractional anisotropy signal and orientation signal to exclude background regions.

3.1 Root dentine

Figure 4a shows a raw transmission image of the tooth sample obtained with the sandpaper modulator. The tooth fragment, a mid-section of the root (figure 2), is manually rotated by 90° and then placed on a holder. The extracted absorption image is presented in figure 4b. The mean scattering is shown in figure 4c. The main orientation (figure 4d) is represented using the eigenvectors of the 2D scattering tensor with the shortest length using an HSV color scheme, where the hue (color shade) indicates fiber orientation projected onto the detector plane, the saturation represents the fractional anisotropy, and the value (brightness) reflects the mean scattering intensity.

We hypothesize that the scattering signal primarily originates from the dentinal tubules. As the tubules move toward the outer regions of the tooth, their density decreases. This explains why there is an enhancement in the central area of the sample in the mean scattering signal (figure 4c). It is important to highlight that these tubular structures are not resolved and remain invisible in the absorption signal (figure 4a).

In figure 5 two tomographic slices (sagittal, and coronal respectively) through the tooth sample are shown. Although dentine tubules are not directly visible in the absorption signal, they generate scattering signals that provide insights into the local microstructure. The main-orientation signal confirms the expected orientation of the dentinal tubules, which run from the dentine enamel junction to the dentine pulp border. Secondary dentine might be responsible for the changing orientation towards the center (pulp chamber). In figure 5 the reconstructed tubules are aligned along the central axis of the tooth (red, x axis) in the central region and fan out toward the surface in the peripheral area (green, z axis, and blue, y axis). Despite the archaeological origin of the tooth sample, the general strong directionality of fibers is visible in the acquired data.

2025 JINST 20 C02028

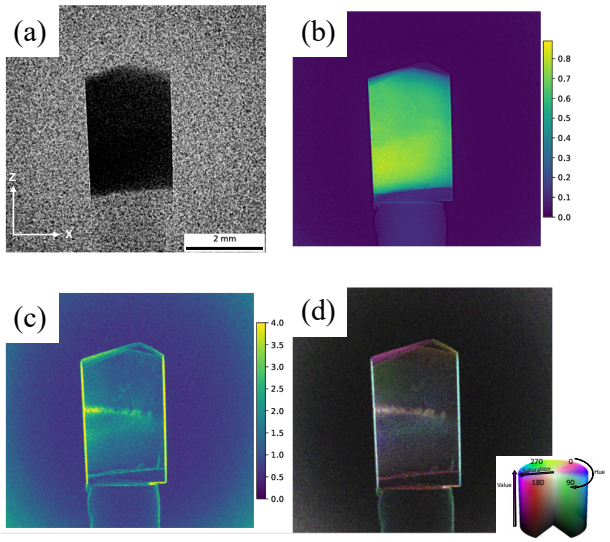

Figure 4. (a) An example of one of the projections of the tooth sample with a sandpaper modulator at $\alpha = 0°, \beta = 0°$. The sample is rotated by 90° with respect to the position reported in figure 2. (b) Extracted absorption image, (c) mean scattering in arbitrary units and (d) main orientation signals. Each pixel corresponds to a unique region of the input image covered by overlapping windows (5×5 pixels).

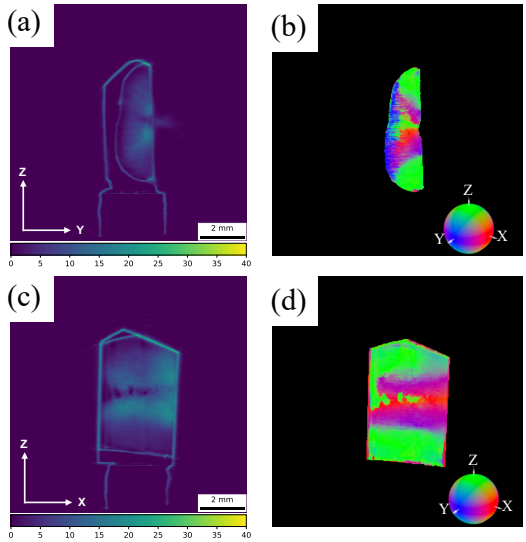

Figure 5. Two slices through the tomographic volume of the tooth fragment. A sagittal slice of the tooth: (a) mean scattering signals in arbitrary units, (b) main orientation signals, where the color is an RGB representation of the local structure orientation. The color ball is symmetric with respect to the $x-y$, $x-z$, and $y-z$ planes. A coronal slice of the tooth: (c) mean scattering signals in arbitrary units, (d) main orientation signals.

3.2 Cortical bone

Figure 6a shows a raw transmission image of the femur sample obtained with the sandpaper modulator. The extracted absorption image is presented in figure 6b. The mean scattering (figure 6c) is calculated as the mean of the eigenvalues of the scattering tensor. From the main orientation signal of this projection (figure 6d), it is visible how the main orientation is along the main axis of the sample (cyan color), as expected from a femur fragment.

In figure 7, a coronal slice through the reconstructed volume of the femur fragment is shown. The interpretation of the extracted orientations (figure 7d) in this sample is not obvious. In these preliminary results, we were able to measure a signal and therefore an information about the sample. Due to the complex and hierarchical nature of bone and possible bone remodeling occurring in the measured specimen, it is not clear yet where this signal is originating from. For such complex materials, a more systematic approach with better known bone samples and validation is necessary to first understand the origin of the signal and possibly moving to more complex cases. However, from the scattering anisotropy signal (figure 7b) and especially from the mean scattering signal (figure 7c) it is possible to identify the cement lines (white arrow), interfaces between the osteons and the bone matrix, as vertical lines with a stronger scattering signal compared to the rest of the bone.

2025 JINST 20 C02028

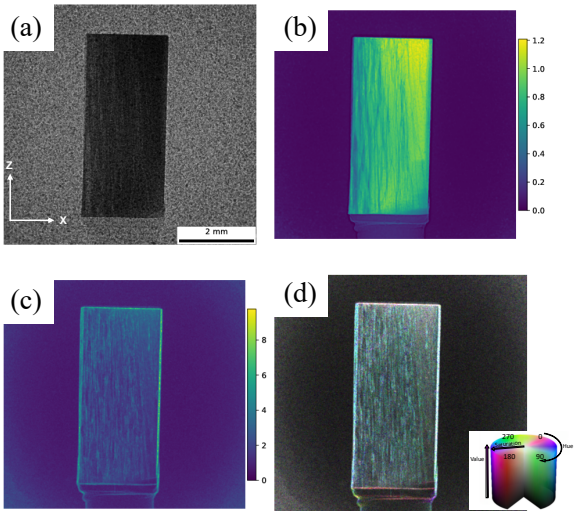

Figure 6. (a) An example of one of the projections of the femur sample with a sandpaper modulator at $\alpha = 0°$, $\beta = 0°$. (b) Extracted absorption image, (c) mean scattering in arbitrary units and (d) main orientation signals.

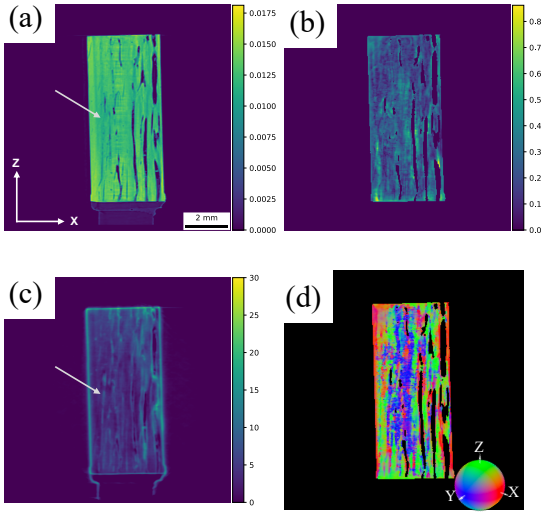

Figure 7. A coronal slice through the tomographic volume of the femur fragment. (a) Extracted absorption, (b) scattering anisotropy in arbitrary units and (c) mean scattering signals in arbitrary units are shown. (d) Orientation signals, where the color is an RGB representation of the local structure orientation. The white arrow indicates one cement line.

4 Conclusions

In conclusion, tensor tomography has the potential to generate detailed 3D reconstructions of microstructural features in biological tissues, such as dentinal tubules in teeth, but also demonstrates its limitations.

In the dental sample, we reconstructed the orientation and the distribution of dentinal tubules, key determinants of dentine's mechanical properties. These tubules differ in size, density, and arrangement between species and can be influenced by physiological or environmental stress. By analyzing the directional characteristics of dentine's anisotropic structure, tensor tomography could contribute to the understanding of differences in the feeding behaviors of different species. For example, a change in dentine structure could indicate adaptation to tougher diets, which could be compared between different hominin species or across periods. The method could also have clinical dentistry applications. As highlighted by Zaslansky et al. [16], understanding the 3D structure and orientation of dentine tubules could enhance restorative procedures and improve simulations of teeth's mechanical properties, as well as for palaeopathology and oral health.

In addition, the first attempt of tensor tomography with cortical bone is presented. The interpretation of the extracted orientations in this sample presented challenges due to its complex microstructure [17]. The imaged bone fragment, derived from an adult individual, consisted of remodeled lamellar bone with high osteon density and lacked woven bone. Due to the changes and layering of the orientation along the axis of the bone and the nanoscale sizes of the collagen fibers, a more systematic approach with better known bone samples and validation is necessary to first understand the origin of the signal in order to visualize features of relevance.

2025 JINST 20 C02028

Overall, this study illustrates some potentials and limitations of tensor tomography for analyzing the microstructural organization of archaeological human tissues. Further advancements, such as increased resolution and a reliable reconstruction of multiple overlapping scattering orientations within a single analysis window, could significantly enhance the versatility and robustness of tensor tomography. These developments would make the method even more valuable for both archaeological research and clinical applications.

Acknowledgments

We acknowledge the European Synchrotron Radiation Facility (ESRF) for provision of synchrotron radiation under proposal number $MD1413$. This publication is part of a project that has received funding from the European Research Council (ERC) under the European Union's Horizon 2020 research and innovation program (Grant agreement No. 866026). S.A.M. Lemmers acknowledges the support of the EC-Marie Skłodowska-Curie Actions (HORIZON-MSCA-2021-PF-01-01, ENIGMA, GA 101065448).

Data and code availability. The data and the code that support the findings of this study are available from the corresponding author upon reasonable request.

References

[1] F. Schaff et al., *Six-dimensional real and reciprocal space small-angle X-ray scattering tomography*, *Nature* **527** (2015) 353.

[2] M. Liebi et al., *Nanostructure surveys of macroscopic specimens by small-angle scattering tensor tomography*, *Nature* **527** (2015) 349.

[3] Z. Gao et al., *High-speed tensor tomography: iterative reconstruction tensor tomography (IRTT) algorithm*, *Acta Cryst.* **75** (2019) 223.

[4] A. Malecki et al., *X-ray tensor tomography*, *EPL* **105** (2014) 38002.

[5] J. Vogel et al., *Constrained X-ray tensor tomography reconstruction*, *Opt. Express* **23** (2015) 15134.

[6] T.H. Jensen et al., *Directional x-ray dark-field imaging*, *Phys. Med. Biol.* **55** (2010) 3317.

[7] J. Kim, M. Kagias, F. Marone and M. Stampanoni, *X-ray scattering tensor tomography with circular gratings*, *Appl. Phys. Lett.* **116** (2020) 134102.

[8] J. Kim et al., *Fast acquisition protocol for X-ray scattering tensor tomography*, *Sci. Rep.* **11** (2021) 23046.

[9] J. Kim et al., *Tomographic Reconstruction of the Small-Angle X-Ray Scattering Tensor with Filtered Back Projection*, *Phys. Rev. Appl.* **18** (2022) 014043.

[10] G. Lautizi et al., *Universal reconstruction method for x-ray scattering tensor tomography based on wavefront modulation*, *Phys. Rev. Appl.* **22** (2024) 024031 [arXiv:2406.18680].

[11] G. Lautizi et al., *Robust dark-field signal extraction for modulation-based x-ray tensor tomography*, *Appl. Phys. Lett.* **125** (2024) 264103 [arXiv:2411.18482].

[12] A. Nanci, *Ten Cate's Oral Histology*, Elsevier Health Sciences (2017).

[13] C. Dean, *How the microstructure of dentine can contribute to reconstructing developing dentitions and the lives of hominoids and hominins*, *Comptes Rendus Palevol* **16** (2017) 557.

2025 JINST 20 C02028

[14] S.A.M. Lemmers et al., *Burned Fleshed or Dry? The Potential of Bioerosion to Determine the Pre-Burning Condition of Human Remains*, *J. Archaeol. Method Theory* **27** (2020) 972.

[15] P.J. Basser and C. Pierpaoli, *Microstructural and Physiological Features of Tissues Elucidated by Quantitative-Diffusion-Tensor MRI*, *J. Magn. Reson. B* **111** (1996) 209.

[16] P. Zaslansky, S. Zabler and P. Fratzl, *3D variations in human crown dentin tubule orientation: A phase-contrast microtomography study*, *Dent. Mater.* **26** (2010) e1.

[17] K.E. Stockhausen et al., *Collagen Fiber Orientation Is Coupled with Specific Nano-Compositional Patterns in Dark and Bright Osteons Modulating Their Biomechanical Properties*, *ACS Nano* **15** (2021) 455.

2025 JINST 20 C02028